

See discussions, stats, and author profiles for this publication at: <https://www.researchgate.net/publication/224938128>

Initiation of the Reaction of Deamidation in Triosephosphate Isomerase: Investigations by Means of Molecular Dynamics Simulations

ARTICLE in THE JOURNAL OF PHYSICAL CHEMISTRY B · MAY 2012

Impact Factor: 3.3 · DOI: 10.1021/jp3013305 · Source: PubMed

CITATIONS

3

READS

34

3 AUTHORS:



İlke Uğur

Technische Universität München

9 PUBLICATIONS 96 CITATIONS

[SEE PROFILE](#)



Viktorya Aviyente

Bogazici University

146 PUBLICATIONS 1,447 CITATIONS

[SEE PROFILE](#)



Gérald Monard

University of Lorraine

41 PUBLICATIONS 964 CITATIONS

[SEE PROFILE](#)

Initiation of the Reaction of Deamidation in Triosephosphate Isomerase: Investigations by Means of Molecular Dynamics Simulations

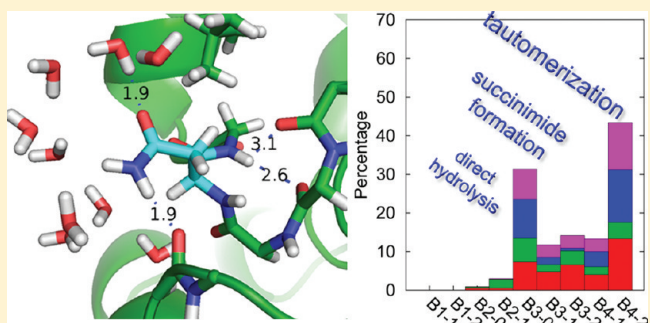
Ilke Ugur,^{†,‡} Viktorya Aviyente,[†] and Gerald Monard^{*,‡}

[†]Department of Chemistry, Boğaziçi University, 34342 Bebek, Istanbul, Turkey

[‡]Theoretical Chemistry and Biochemistry Group, SRSMC, Lorraine University, CNRS, Boulevard des Aiguillettes B.P. 70239, F-54506 Vandoeuvre-les-Nancy, France

S Supporting Information

ABSTRACT: Deamidation of asparagine is the spontaneous degradation of this residue into aspartic acid. The kinetics of this slow reaction is mainly dependent on the nature of the adjacent amino acid that follows asparagine in a peptide or protein primary sequence. In the homodimer triosephosphate isomerase (TPI), there are two main deamidation sites per subunit: Asn15–Gly16 and Asn71–Gly72 for which deamidation dynamics are known to be interrelated. In this study, we investigate the initiation of the deamidation reaction in TPI by means of molecular dynamics. Simulations based on classical AMBER force field are performed in a 60 to 90 ns time scale for six distinct samples. Conformational changes, desolvation effects, and hydrogen bond networks are analyzed to interpret the experimental findings and previous quantum mechanical (QM) results. Results that are based on desolvation analysis clarify the assignments in the literature about the different behaviors of two deamidating sites in TPI. Conformational analysis supports findings suggested by QM studies: the most favorable reaction mechanism is the one that yields to succinimide intermediate via one or two step routes. The mechanism leading to the succinimide intermediate most likely involves the formation of a tetrahedral intermediate that is formed either directly from asparagine or via a side chain tautomer intermediate. In all cases, surrounding water molecules are present to assist the reaction.



1. INTRODUCTION

Deamidation is the conversion of the neutral amide side chain to the negatively charged carboxylate. Among the 20 neutral amino acids, asparagine (Asn) and glutamine (Gln) residues are known to undergo spontaneous nonenzymatic deamidation to form aspartic acid (Asp) and glutamic acid (Glu) residues under physiological conditions.^{1–5} This reaction is of significant biological interest because it causes time dependent changes in conformation and limits the lifetime of peptides and proteins. Deamidated proteins have been found in some aged and diseased tissues, such as human eye lens cataracts⁶ and Alzheimer's plaques.⁷ The timed processes of protein turnover, development, and aging have been suggested as possible roles for deamidation.⁸ Robinson et al. have proposed the molecular clock hypothesis, which suggests that deamidation is a biological molecular timing mechanism that could be set to any desired time interval by genetic control.⁹ Furthermore, they proposed that the instability of asparaginyl and glutaminyl residues is their primary biological function and that they serve as easily programmable molecular clocks.⁹ Recent experiments^{10–16} and computations^{17–22} have been in accord with this hypothesis and provided compelling evidence of its significance.

Some peptides and proteins, which are of special interest in the development of knowledge about deamidation, have been studied more thoroughly. In this study, mammalian triosephosphate isomerase (TPI) is chosen to elucidate the deamidation of asparagine by using molecular dynamical (MD) tools. This enzyme is biologically important and also has special features in order to investigate deamidation reactions. It is a homodimeric enzyme that can be found in almost all of the living organisms ranging from bacteria to mammalian. It rapidly and reversibly converts dihydroxyacetone phosphate (DHAP) into glyceraldehyde-3-phosphate (GAP) in the glycolytic pathway. The enzyme is only active in the dimeric form, which consists of identical monomers of 246 residues. The monomers are folded as TIM-barrel, which is built by eight α -helices on the outside, eight parallel β -strands on the inside, and eight loops referred to as loop1 to loop8.^{23,24}

It has been shown that mammalian TPI deamidation occurs preferentially at two distinct asparagines: MetAsn(15)Gly (on loop1) and ThrAsn(71)Gly (on loop3).²⁵ A glycine residue next to asparagine is required for a deamidation reaction to occur.

Received: February 9, 2012

Revised: May 8, 2012

Published: May 10, 2012

These residues, Asn(15)Gly and Asn(71)Gly, are juxtaposed to each other and are located at the interface between the two subunits of this dimeric enzyme (Figure 1).

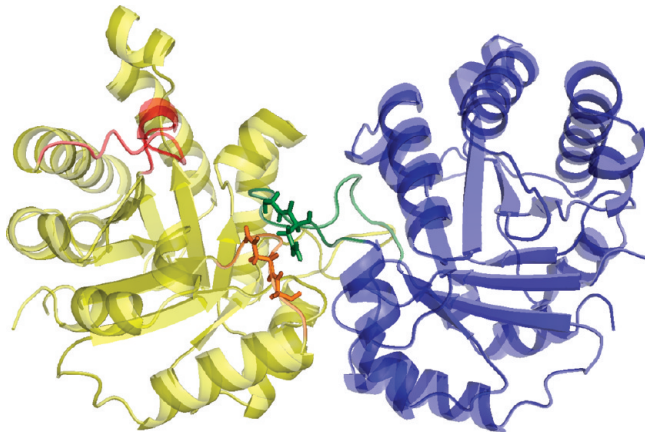


Figure 1. Cartoon representation of the TPI dimer. Two identical monomers A and B are represented by blue and yellow, respectively. Loop6 is in the closed conformation in monomer A and colored in red. Loop1 from monomer B, which contains Asn15Gly16, and loop3 from monomer A, which contains Asn71Gly72, are colored in orange and green, respectively. AsnGly residues are shown as sticks to emphasize the intermolecular interactions between the two deamidation sites.

Gracy et al. have indicated that Asn71 deamidates earlier than Asn15,²⁵ so that the ThrAsn(71)Gly is named as primary

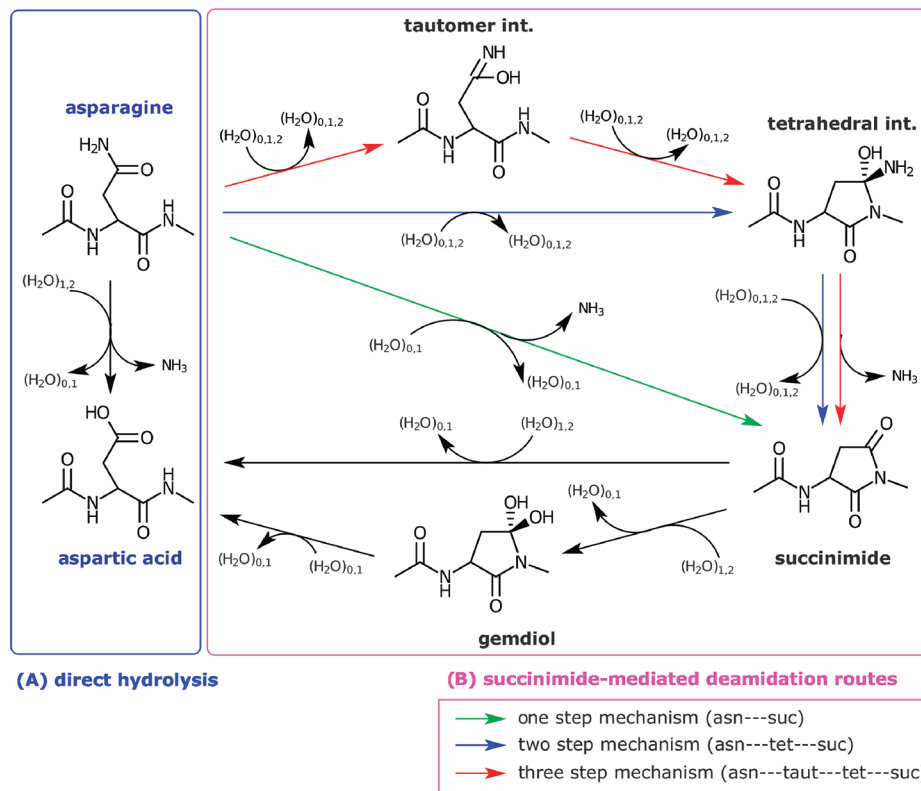
deamidation site and that the MetAsn(15)Gly is the secondary deamidation site. They also suggest that the deamidation of Asn71 is a prerequisite for the deamidation of the juxtaposed Asn15 on the neighboring subunit.²⁵ However, the deamidation coefficient (C_D) values of Asp71/Asp15 was computed as 2.27:1,¹⁶ which is in agreement with the results obtained by characterization of TPI deamidation products, 2.54:1 for human and 1.73:1 for rabbit TPI,²⁶ so that these two deamidations can also be considered as independent events.¹⁶

On the basis of conclusions derived from several experiments, Robinson et al. reported that small peptides deamidate more rapidly than proteins and also that the secondary and tertiary structure of the enzyme has an essential impact on deamidation.¹⁶ In the case of human TPI, the half-life of the deamidation is found as 21.7 days at pH 7, 37 °C.²⁷ For a pentapeptide that has the Val–Ser–Asn–Gly–Val sequence, the half-life is determined as 5.8 h under the same experimental conditions.²⁸

In each monomer of TPI, loop6 (residues 166 to 176) has a particular physiological function: this 11-residue loop region moves more than 7 Å and closes over the active site when the substrate binds and a hinge-type motion takes place. As the enzyme functions, a hinged lid over the active site closes, excluding water and preventing hydrolysis of triosephosphates to toxic products. Gracy et al. also suggest that, when the lid is closed, Asn71 in that monomer deamidates more readily (Figure 1).²⁵

Capasso et al. have proposed that deamidation of relatively unrestrained Asn residues goes through a succinimide

Scheme 1. Summary^{29–31} of the Previously Suggested Mechanisms for the Conversion of Asparagine in Aspartic Acid^a



^aBlack route (A): direct hydrolysis of asparagine to aspartate; green route, direct conversion from asparagine to a succinimide intermediate (one step mechanism); blue route, formation of a succinimide intermediate via a tetrahedral intermediate (two steps mechanism); red route, tautomerization of asparagine followed by the formation of a tetrahedral intermediate, then of a succinimide intermediate (three steps mechanism). All succinimide-mediated deamidation routes (B) include a concerted or step-wise hydrolysis of the succinimide intermediate in aspartate.

intermediate.^{10–12} Quantum mechanical (QM) studies carried out by some of us have suggested that the deamidation at neutral pH can proceed through various mechanisms (see Scheme 1).^{17–19,29–31} Detailed discussions of these mechanisms will be provided in what follows.

In this article, we explain the relationship between two deamidation sites, loop6 motion, and substrate binding using classical force field and molecular dynamics techniques. All-atom molecular dynamic simulations are performed in a 60 to 90 ns time scale for six distinct samples to interpret the experimental findings and the QM results. Deamidation of Asn residues is examined based on the configurational changes during the simulation. Considering the accelerating effect of solvation of Asn residues on deamidation, the differences of the desolvation of the residues and the hydrogen bonding networks are analyzed. The plausible reactive conformers suggested earlier in QM studies, including water assisted mechanisms, are also examined.

2. COMPUTATIONAL DETAILS

2.1. Preparation of the Samples. The crystal structure of the rabbit muscle TPI (PDB code 1R2R, resolution 1.5 Å³²) was used as the starting structure of the simulations. This structure is apo and contains two identical dimers. The active site loop (loop6) in one of the four subunits of 1R2R is in the closed conformation. For simplicity, one of the dimers was deleted, and the dimer with one monomer that has the active site loop in the closed conformation was kept. The final structure of the TPI is a dimer in which the active site loop is open in one of the monomers and closed in the other. The monomer with active site loop open is named as monomer A, and the one with the closed loop is monomer B. This nomenclature is used to label the loops and the residues regarding the corresponding monomer (loopA1 or loopB1, AsnA71 or AsnB71, etc.).

Our basic concern was to understand the differences between the deamidations of Asn71 and Asn15 and to investigate the effect of motion of loop6 and substrate on deamidation. On the grounds of our concerns, six distinct samples, based on the 1R2R structure, were prepared. The nomenclature of the samples is as follows (Table 1):

Table 1. Nomenclature of the Samples

name	monomer A		monomer B	
	residue71	loop6	residue71	loop6
WOW	N	open	N	closed
CC	N	closed	N	closed
OO	N	open	N	open
CS	N	open	N	closed
AASP	N71D	open	N	closed
BASP	N	open	N71D	closed

WOW: It is a wild type apo dimer TPI in which loopA6 is open and loopB6 is closed. This sample was prepared by keeping the exact structure of the crystal of the dimer of 1R2R.

CC and OO: These samples were prepared to examine the effect of motion of the active site loop on deamidation. The closed structure of loopB6 is copied, and the loopA6, which has the open structure, was replaced with this copied closed loop. Both of the loop6's were kept closed at the beginning of the simulation (sample CC). The reverse of this procedure was performed to obtain the sample in

which both loop6s were kept open at the beginning of the simulation (sample OO).

CS: To understand the effect of substrate, one ligand-bound sample was prepared by using DHAP as the ligand. DHAP conformation inside the TPI active site was extracted from Yeast TPI structure (PDB code 1NF0,³³ resolution 1.2 Å) and incorporated into the active site of monomer B of 1R2R by active site structure fitting. According to a Needleman–Wunsch sequence alignment comparison method,³⁴ 1R2R and 1NF0 share 50% identical residues and have 67% sequence similarity. Fitting of the identical residues between both structures gives an all atom rms of 1.159 Å using the McLachlan algorithm as implemented in the ProFit software.³⁵ 1R2R and 1NF0 respective active sites contain identical residues (i.e., Lys 12, His 95, Glu 165, Gly 232, and Gly 233) with very similar three-dimensional structure. The rms between both binding sites is evaluated at 0.232 Å by ProFit.³⁵

AASP and BASP: Two mutant samples were prepared to investigate the effect of Asp71 on Asn15. Asn71 was mutated to Asp71 in monomer A (sample AASP) and in monomer B (BASP). The mutations were performed by simply patching Asp on Asn.

One sample, with the substrate in the open loopA6, was also prepared and simulated up to 100 ns to observe the effect of the substrate. However, the substrate left the active site at the very beginning (4 ns) of the simulations, so this sample is discarded, and the results regarding this sample are not discussed in this article.

2.2. Molecular Dynamics Simulations. The systems were hydrogenated, and the topology and coordinate files were built with the tLEAP module of AMBER 9.³⁶ Molecular dynamics simulations were performed using the program AMBER with the ff03 force field parameters.³⁷ The protonation states of histidine residues were determined according to their polar environment. Samples WOW, CC, and OO were neutral. CS, AASP, and BASP had –2, –1, and –1 charges, respectively, and counter sodium ions were added to neutralize these systems. Waters from the crystal structure were deleted, and the systems were solvated with explicit TIP3P water molecules.³⁸ The resulting systems are cubic, of edge length 93.13 Å, have an initial density of 1.0, and contain about 24 000 water molecules. This initial setting yields to molecular systems having a protein concentration in each cubic box of about half the 1R2R crystal concentration.

The simulations were done using the SANDER module of AMBER 9. An NVT sample was used with Andersen temperature coupling.³⁹ Periodic boundary conditions were imposed on the systems. The particle mesh ewald summation technique⁴⁰ was used with a cutoff distance of 8 Å. A time step of 1.5 fs was used by the implementation of the SHAKE algorithm⁴¹ for the bonds involving hydrogens.

The equilibration of the systems was performed in a four stage process. First, only the hydrogen atoms of the system were allowed to move during a 15 ps long molecular dynamics using a strong temperature coupling (i.e., velocities were randomly updated every 10 steps). This was to ensure a proper geometry of the protein hydrogen atoms that were added by the tLEAP program and to relax the hydrogen bond network between the water molecules and the protein. Second, the whole system was simulated for another 15 ps with the same strong temperature coupling, but here, all atoms were allowed to move. Third, a subsequent 100 K molecular dynamics was performed with

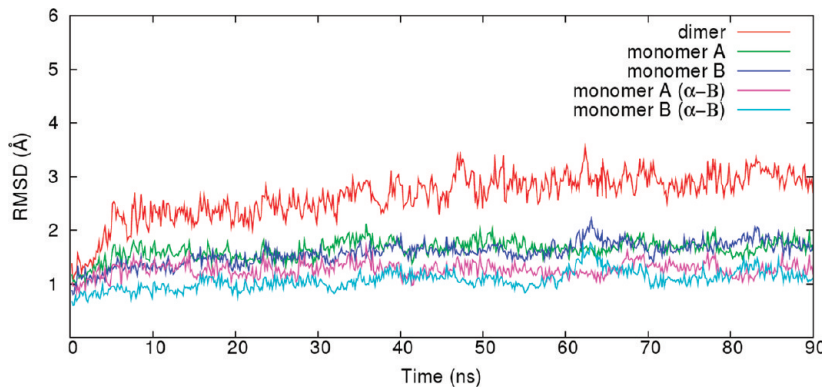


Figure 2. Variations of the rmsd (in Å) along the molecular dynamics trajectory (in ns) using 1R2R crystallographic structure as a reference. Rmsd are computed for the complete dimer structure (red), monomer A only (green), monomer B only (blue), all α helices and β sheets of the subunit A (magenta), and all α helices and β sheets of the subunit B (cyan), respectively.

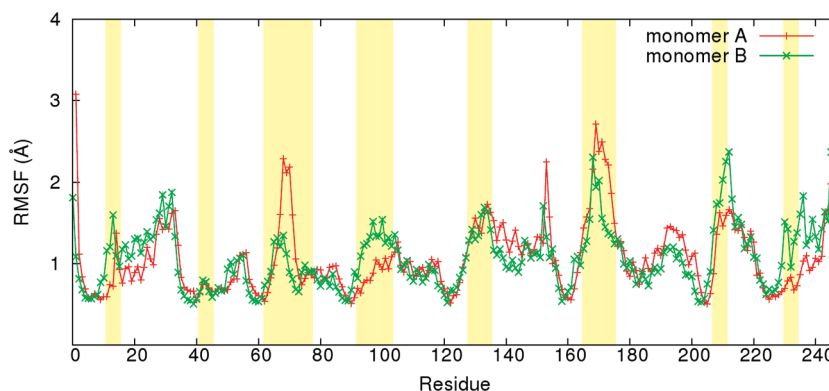


Figure 3. Atomic fluctuations (RMSF: root-mean-square fluctuations of C α atoms) for the sample WOW. Yellow shading indicates the loops of the TIM barrel.

looser temperature coupling (i.e., velocities were randomly assigned every 50 steps). Fourth, the thermostat temperature was increased to 300 K, and another 15 ps molecular dynamics was performed using the same previous temperature coupling. Finally, productions were performed at 300 K using standard Andersen thermostat as implemented in AMBER 9 (i.e., with atomic velocities updated every 1000 steps). The samples WOW and BASP were simulated up to 90 ns, and the remaining samples up to 60 ns at the same temperature.

2.3. Trajectory Analysis. The root-mean-square deviation (rmsd) results were calculated by using the ProFit software.³⁵ Atomic fluctuation (AF) calculations and hydrogen bond analysis were performed by using the ptraj module of Amber 9. Generation of the plots was done using Gnuplot 4.2.⁴²

3. RESULTS AND DISCUSSION

3.1. Stability of the Trajectories. To investigate the stability of the trajectories, the root-mean-square deviation of C α atoms has been computed (see Figure 2 for WOW and Supporting Information for other samples). For all samples, the reference structure corresponds to the initial structure of the molecular dynamics (e.g., the X-ray structure for WOW). The rmsd value increases moderately along the simulation to reach a rather high average value of \sim 3–3.5 Å. By distinctly computing the rmsd of each monomer, it can be seen that each monomer does not unfold and keeps a low rmsd value along the trajectory at \sim 1.5–2 Å. This indicates that the motions of the monomers with respect to each other are at the origins of the large backbone

deviations in TPI. This behavior has been investigated earlier.⁴³ Considerable high values of the rmsd of the dimeric protein can be explained by those intramonomer motions. Our findings are compatible to what have been reported in other publications. Details of the investigations of those motions will not be discussed since they are out of context. Given that rmsd values of the distinct monomers or alpha helices and beta sheets stay within a 0.5–2 Å range, we consider our simulations as stable.

The atomic fluctuations based on the C α atoms with respect to the residues are calculated (Figure 3). For all samples, residues on helices and beta sheets of the TPI barrel fluctuates less than the residues on the loops. The secondary structure of the protein is conserved during the simulation. Excluding the terminal ends of the protein, most flexible residues are the hinges of the catalytic loops, loop1, 2, ..., loop8 (colored in yellow in Figure 3). Residues between 30–32 and 141–150, which are located on the stability loops of the TPI barrel, also have some flexibility. Loop6 and loop7, which are known as the most flexible loops of TPI,⁴⁴ have the highest fluctuation values for all of the samples. These results also show the reliability of the simulations.

3.2. Solvent Accessibility. **3.2.1. Desolvation Effects on Residues Asn and Gly.** Reaction paths leading to deamidation of Asn residue imply the deprotonation of the peptidic N–H group adjacent to Asn to form a succinimide ring. In the case of TPI, it corresponds to the N–H group of Gly16 and Gly72, respectively, bound to Asn15 and Asn71. The capability for the proton of this N–H group to leave glycine and to help the formation of the succinimide ring can be related to the pK_a of the nitrogen involved in the peptide bond. There is no experimental

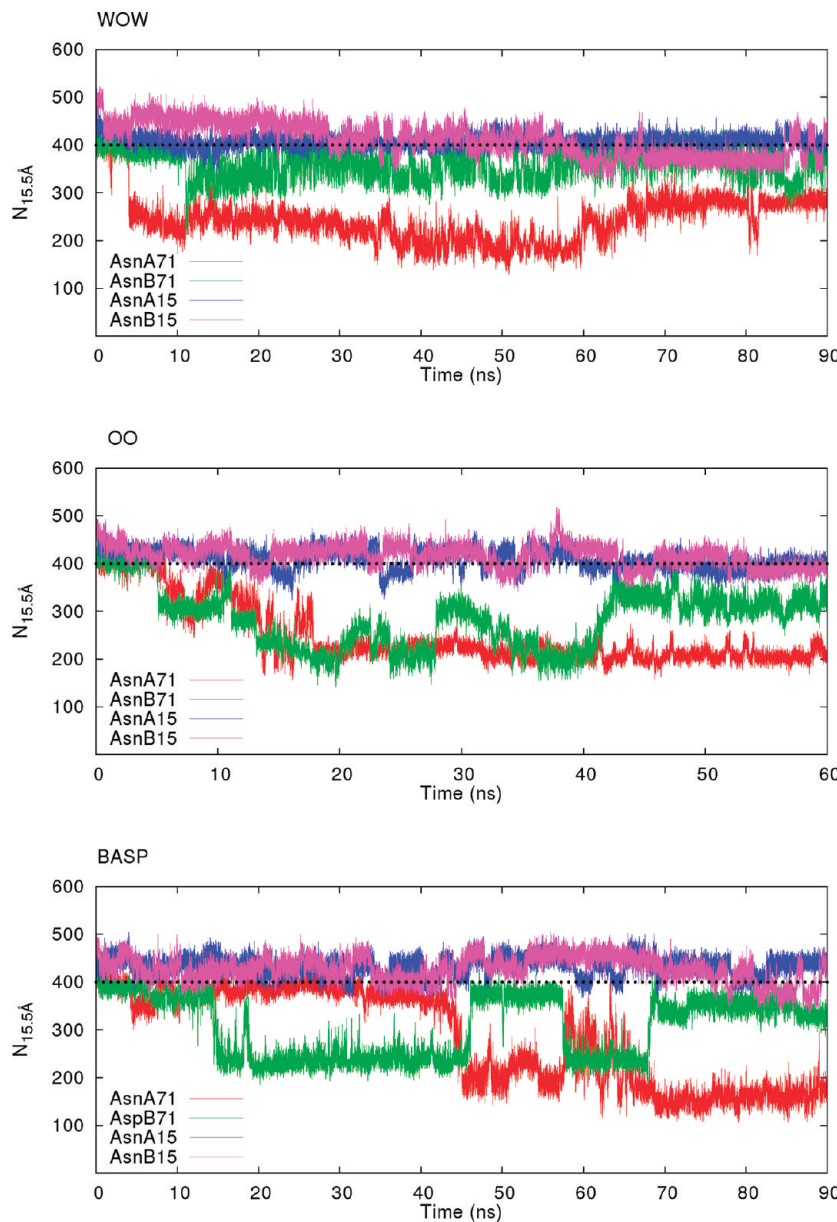


Figure 4. $N_{15.5\text{\AA}}$ of Asn with respect to time (Asn 15A, 71A, 15B, and 71B are depicted in blue, red, magenta, and green, respectively).

measurement of such a pK_a , but theoretical considerations can be brought on its variations with respect to local protein environment. Additionally, the peptidic side chain of Asn can also be recipient for protons, depending on the considered deamidation reaction mechanism. In the PROPKA program that has been developed to estimate pK_a s of ionizable protein side chains by Li et al.,⁴⁵ the pK_a of an ionizable residue is perturbed from its standard aqueous state by different factors: desolvation, hydrogen bonding, and charge–charge interactions.⁴⁵ In this study, pK_a shift values due to desolvation of the Asn and Gly residues, located at the four deamidation sites, are calculated by using the equations proposed by Li et al.⁴⁵ The calculations of pK_a shifts of Asn and Gly are based on model residues, Asp and Arg respectively, and parameters are adopted as follows: (i) Asn71@CG, Asn15@CG, Gly72@N, and Gly16@N are chosen as center of ionizable groups; (ii) local radii (R_{local}) are determined as 4.5 Å and 5 Å, respectively, in agreement with typical R_{local} used by Li et al.;⁴⁵ (iii) pK_a shifts are calculated using the following equations:

Local ($\Delta pK_{\text{LocalDes}}$):

$$\Delta pK_{\text{LocalDes}} = N_{\text{local}} C_{\text{local}} \quad (1)$$

where N_{local} is the number of non-hydrogen protein atoms within a distance R_{local} to the center point of the ionizable group, and C_{local} is a parameter representing the contribution of each neighbored atom to the local desolvation effect. The latter parameter is constant pK_a shift per atom taken as 0.07, as suggested by Li et al.⁴⁵

Global ($\Delta pK_{\text{GlobalDes}}$):

$$\Delta pK_{\text{GlobalDes}} = (N_{15.5\text{\AA}} - 400) C_{\text{global}} \quad (2)$$

where, $N_{15.5\text{\AA}}$ is the number of non-hydrogen protein atoms within 15.5 Å of the center of the ionizable group, $N_{15.5\text{\AA}} - 400$ is the excess of protein atoms, $C_{\text{global}} = 0.01$.

Total (ΔpK_{Des}):

$$\Delta pK_{\text{Des}} = \Delta pK_{\text{GlobalDes}} + \Delta pK_{\text{LocalDes}} \quad (3)$$

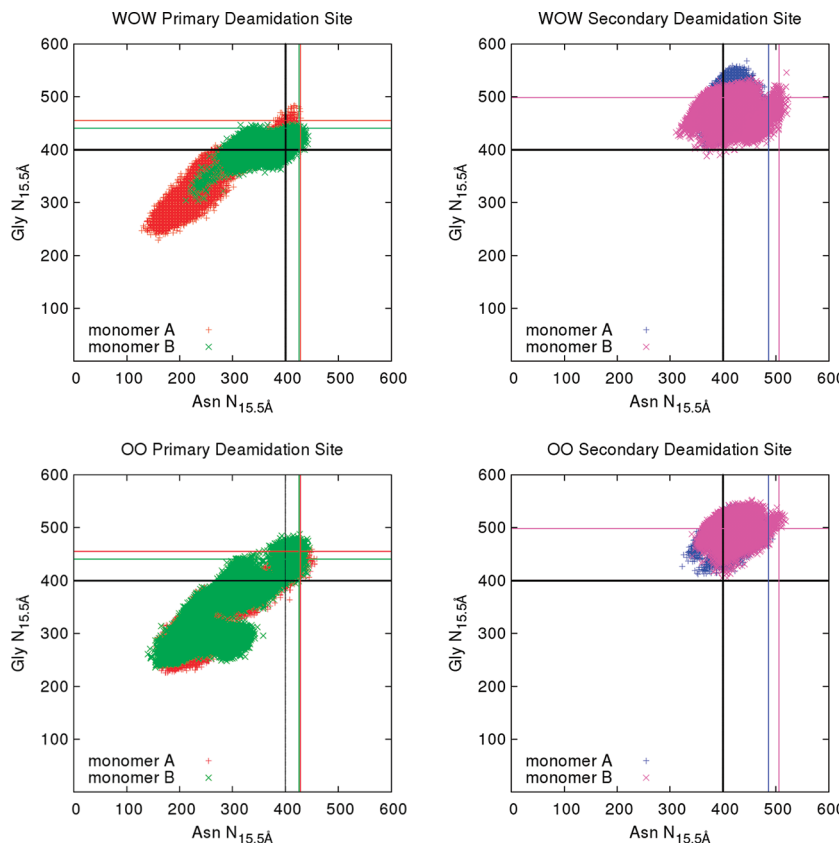


Figure 5. $N_{15.5\text{\AA}}$ of Asn vs Gly results. (Asn A15, A71, B15, and B71 are depicted in blue, red, magenta, and green, respectively. $N_{15.5\text{\AA}}$ of the crystal structure is shown with lines).

All the parameters used to compute the desolvation effect (i.e., C_{local} , C_{global} , R_{local} , and the 15.5 Å global radius) are chosen according to the discussions made by Li et al.⁴⁵ It is suggested that these constants give the best results to mimic desolvation effects on pK_a deviations. In the original PROPKA formulation, only the non-hydrogen protein atoms outside the considered amino acid are counted. This is justified since only side chain ionizable groups are considered. In our case, since some ionizable groups are peptidic groups, we counted all non-hydrogen protein atoms within R_{local} or 15.5 Å of the center atoms and subtracted to N_{local} and $N_{15.5\text{\AA}}$, respectively, a constant minimal number of non-hydrogen atoms. In our study, we subtracted 9 and 10 for Asn and Gly residues, respectively. Variations of $N_{15.5\text{\AA}}$ along the simulations are reported in Figure 4.

The changes in the $N_{15.5\text{\AA}}$ values of Asn@CG and Gly@N with respect to time are analyzed to monitor the variations of the global desolvation effects during the simulations. Residues having $N_{15.5\text{\AA}}$ values greater than 400 are classified as buried residues based on the findings of Li et al.⁴⁵ while other residues are named surface residues. In the crystal structure Asn15@CG, Asn71@CG, Gly16@N, and Gly72@N are in the buried form with, respectively, $N_{15.5\text{\AA}}$ values of 486, 428, 499, and 455 in subunit A and 506, 426, 499, and 441 in subunit B.

In WOW, AsnA71@CG goes to the surface state at the very beginning of the simulation and goes back to the buried state after 70 ns of the simulation. AsnB71@CG keeps an almost constant state (i.e., $N_{15.5\text{\AA}}$ between 300 and 400) during the whole trajectory. Gly16@N and Gly72@N follow the same trend as their neighboring residue with higher $N_{15.5\text{\AA}}$ values in both of the monomers (Figure 4).

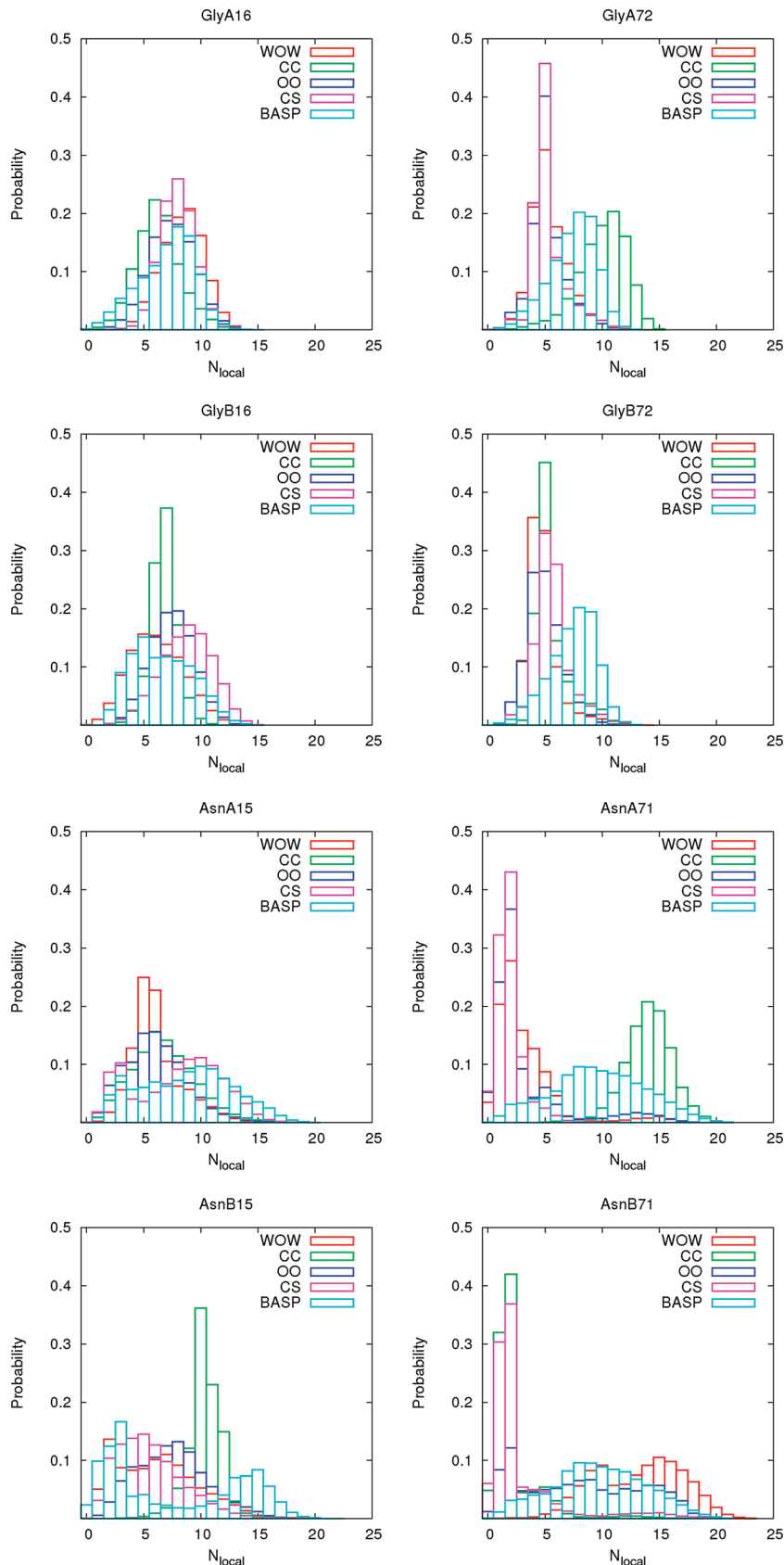
In other samples, both Asn15 side chains keep a buried state as in WOW. In the case of Asn71, trajectories show a change in state for Asn71 with, sometimes, some oscillations between buried and surface states. This is the case for AsnB71 in sample CC; AsnA71 and AsnB71 in samples CS, OO, and BASP; and AsnB71 in sample AASP.

Consequences of the global desolvation investigation show that loop3, which holds the primary deamidation site, can have two stable conformations: solvated and buried. The solvated conformation is different than the crystal structure. However, oscillations between those two conformations especially in WOW and BASP (which are simulated 30 ns longer than the rest) show that both of the conformations are accessible.

For all of the samples, secondary deamidation sites of both subunits always stay in buried conformations with $N_{15.5\text{\AA}}$ values very close to 400 or higher than that. Gly@N has always higher values than Asn@CG, which indicates that Gly is more buried than Asn. It is observed that changes of $N_{15.5\text{\AA}}$ value of Asn@CG and Gly@N are strongly correlated (Figure 5).

Following Li et al. equation for global desolvation, only residues having a $N_{15.5\text{\AA}}$ larger than 400 atoms have their pK_a shifted.⁴⁵ In our samples, $N_{15.5\text{\AA}}$ is always lower for Asn than for its adjacent Gly (see Figure 5); this indicates that the N–H group in glycine residues (16 and 72 in both monomers) are usually more desolvated than the side chains of asparagines. In other terms, Gly is always more buried than Asn.

When comparing Asn15Gly16 vs Asn71Gly72, it is found that Asn15Gly16 usually keeps a buried state along the trajectories, while Asn71Gly72 can be either buried or at the surface of TPI. This means that, in terms of desolvation effect, it will be more difficult to abstract the proton of the peptidic bond between Asn

**Figure 6.** Probability of N_{local} values.

and Gly to form a succinimide intermediate in Asn15Gly16 than in Asn71Gly72 and that the pK_a shift in Gly is higher than the one in Asn.

Figure 6 reports the distribution of the number of neighbors in the local vicinity (N_{local}) of Gly@H and Asn@OD1. We have not found any pattern linking local desolvation to samples'

trajectories. Following Li et al. equation for local desolvation effect, it shows that local environment accounts in average for less than 1 p*K_a* shift unit for all samples.⁴⁵

It has been found experimentally that Asn71 deamidation points to the deamidation of Asn15.²⁵ Molecular dynamics simulations of Asn71 mutated structures (AASP and BASP) can produce some information on the influence of a deamidated residue on the second deamidation site.

Analysis of the correlation of $N_{15,5A}$ between Asn and its adjacent Gly for AASP and BASP trajectories (see Supporting Information) show that the presence of an aspartate residue in position 71 does not change the global desolvation state of the juxtaposed asparagine: the correlation between Asn15 and Gly16 $N_{15,5A}$ numbers are not influenced by a N71D mutation, at least in the time scale of the present simulation.

3.2.2. Hydrogen Bond Analysis. From QM static studies of deamidation on model systems done by Catak et al.,^{29–31} deamidation can occur when a hydrogen bond is formed between the side chain of Asn and the N–H group of the adjacent glycine. A possible descriptor of the reactant state for deamidation can be the formation of a hydrogen bond during the MD simulation between Asn@OD1 and Gly@H (defined hereafter as the hydrogen bond of interest). We report in Table 2 the percent

Table 2. Percent Occupancies of the Hydrogen Bonds of the Sample WOW

Asn OD1…Gly H interaction				
acceptor	donor	% occupancy	distance (Å)	angle (deg)
AsnA15@OD1	GlyA16@H	8.21	2.933	44.73
AsnA71@OD1	GlyA72@H	6.42	3.040	44.87
AsnB15@OD1	GlyB16@H	5.79	2.958	46.50
alternative interactions				
acceptor	donor	% occupancy	distance (Å)	angle (deg)
AsnB71@OD1	AlaB73@H	47.78	3.013	29.20
TrpA12@O	GlyA16@H	20.94	3.260	45.40
TrpB12@O	GlyB16@H	15.70	3.244	39.42
MetA14@O	GlyB72@H	11.56	2.992	23.93

occupancies, during the WOW trajectory, of hydrogen bonds involving Asn@OD1 as a hydrogen bond acceptor. Restrictions are made in Table 2 and, only the percent occupancies of hydrogen bonds involving Asn@OD1 as an acceptor that are higher or equal to the percent occupancy of the respective Asn@OD1…Gly@H hydrogen bond are reported.

During the WOW trajectory, direct hydrogen bonds between Asn@OD1 and Gly@H do not occur frequently. Percent occupancies are low (<10%), and in the case of AsnB71@OD1…GlyB72@H, nearly no hydrogen bond is present. In all cases but for AsnB71, no other hydrogen bond of interest is observed. In contrast, the dominant hydrogen bond interaction for AsnB71 involves AlaB73@H. The specific interaction occurs nearly half of the time during the WOW simulation.

When focusing on the hydrogen bond interactions of Gly@H, one can observe the preferential formation of hydrogen bond with oxygen from the backbone of TPI: GlyA@H interacts more with TrpA12@O, GlyB16@H with TrpB12@O, and GlyB72@H with MetA14@O, respectively. Only GlyA72@H interacts preferentially with AsnA71@OD1.

For all of the samples, the motion of loop3, containing Asn71, can be considered as the main factor that determines these interactions. When loop3 is interrelated with loop1, interactions

between two monomers increase. In sample CC, loop3 of monomer A stays in the buried form. AsnA71@OD1 is bonded to GlyB16@H (Figure 7B), and also, AsnB15@OD1 is bonded

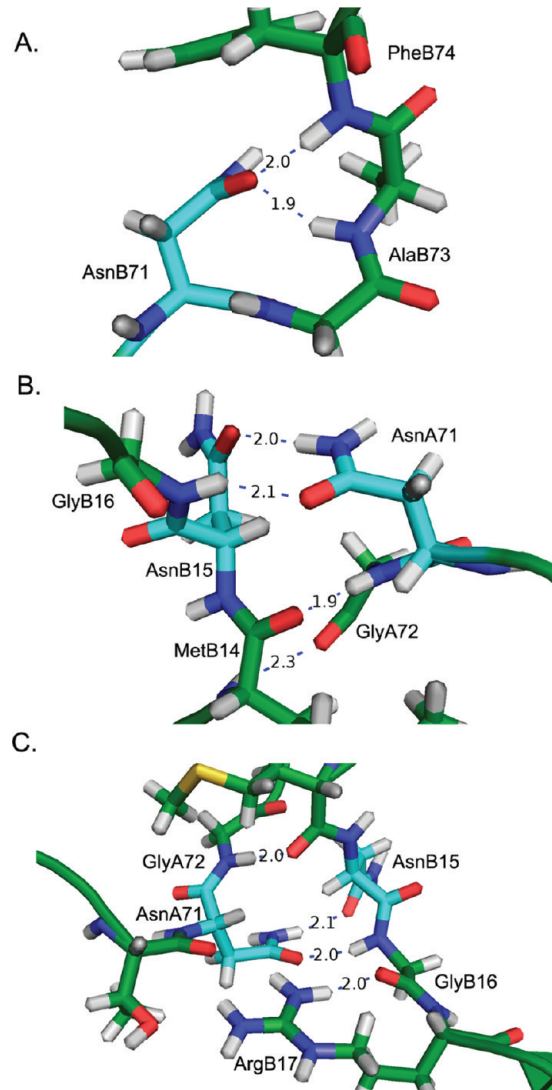


Figure 7. Stable hydrogen bonds ((A) WOW, AsnB71, 34 ns; (B) CC AsnA71 and AsnB15, 5 ns; (C) BASP AsnA71 and AsnB15, 34 ns).

to AsnA71@HD21 with significantly high percent occupancies (76.19 and 67.83, respectively). These kinds of intramonomer interactions cannot be observed in the other samples in which loop3 goes to the solvated form. However, these interactions do not hinder the hydrogen bonds of interest. The occupancy of the hydrogen bond between AsnA71@OD1 and GlyA72@H is found as 10.28 and AsnB15@OD1 and GlyB16@H as 24.69 in the same sample. These percentages are found to be the highest among all of the samples for the computed occupancy. This fact can be explained as follows: when loop3 and loop1 are interrelated, the residues are less flexible so that the hydrogen bonds of interest are also more stable.

From our simulations, we can distinguish three distinctive hydrogen bond acceptors for Gly@H within TPI: Thr70@O for the primary deamidation site, and Trp12@O and Met14@O for the second deamidation site. The former interaction occurs between the TPI monomers, while the latter interactions are intramonomeric.

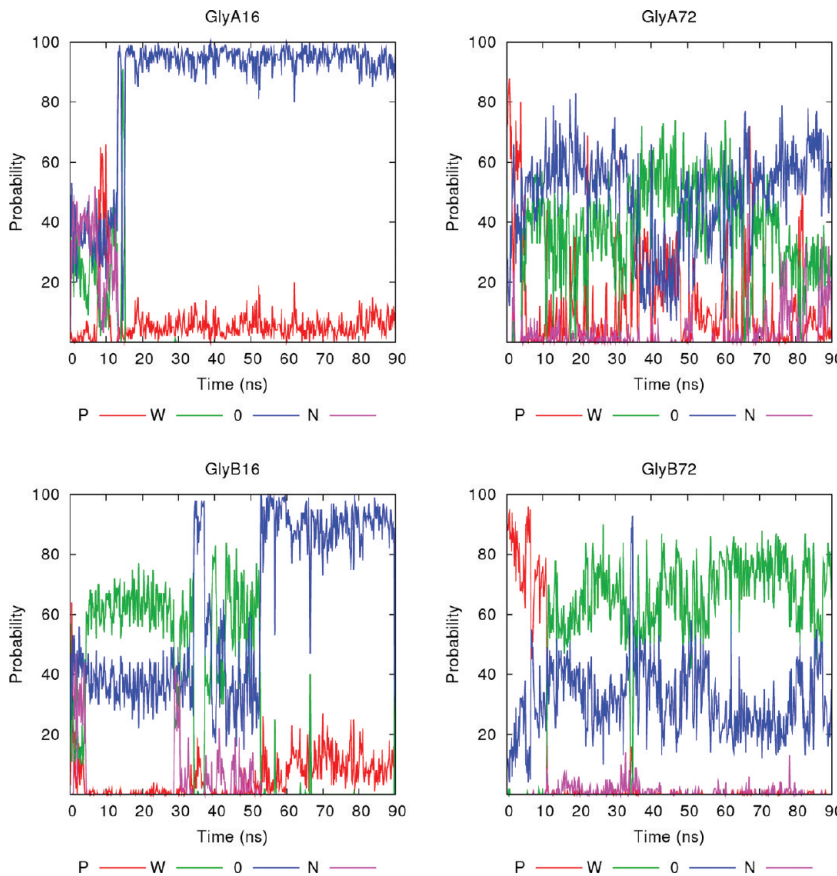


Figure 8. Probabilities of occupancy of Gly H of the sample WOW (red, green, blue, and magenta indicate protein-bound (P), water-bound (W), free (0), and Asn-bound (N) states, respectively).

3.2.3. Gly–H Interactions. Analysis of hydrogen bonding patterns within TPI shows that hydrogen bonds between Asn side chain and its juxtaposed glycine backbone are not the preferential interaction during the MD simulations. Overall, simulations can be analyzed in terms of which kind of hydrogen bond Gly@H can make. Four states are possible for each TPI Gly@H: (1) hydrogen bond to the juxtaposed Asn@OD1 (Asn-bound state); (2) hydrogen bond to another acceptor within TPI (protein-bound state); (3) hydrogen bound to a water molecule (water-bound state); (4) no hydrogen bond at all (free state). MD simulations have been analyzed for consecutive 1.5 ns windows, and percent probabilities for each four possible states have been collected. Evolutions of these probabilities during the WOW trajectory are reported in Figure 8 for each deamidation site Gly@H. The most significant information obtained from this analysis is that the free state is one of the most dominant states during the MD. One example for this fact is GlyA16. Figure 8 depicts that GlyA16 of WOW is desolvated after 12 ns and bonded to neither other residues nor to water up to the end of the simulation.

Figure 9A represents the environment around AsnA15 and GlyA16 for a snapshot at 34 ns of the WOW simulation. There, it can be seen that Gly@H points toward the inner part of the TPI but it does not make any hydrogen bond with TPI residues. The closest hydrogen acceptors are not correctly positioned in terms of distances and angles to form a stable hydrogen bond interaction. A similar free state is observed for the same snapshot for GlyB72 (Figure 9D): an interaction is formed with Met14@SD that is too weak to be considered as a proton bound state.

Among all of the samples, GlyB16 of CC and GlyA72 of BASP are the only examples in which the probability of the protein-bound state is higher than the other states (see Supporting Information). In CC, this state becomes more dominant after 20 ns. In BASP, the probability of having a protein-bond is high at the beginning of the simulation, and this interaction is lost after 42 ns.

The Asn-bound state cannot be considered as a dominant state in any of the samples.

Overall, analysis of the four possible states of Gly@H, as reported Figure 8, shows that Gly@H is mostly in a free state or in interaction with water molecules. To deamidate an Asn residue, Gly@H must not be involved in a stable interaction with a protein residue, other than the adjacent Asn@OD1. This is what we have found for all 4 Gly residues. This means that the proton of the glycine is mostly available during the time of the simulation to participate to a deamidation reaction.

3.3. Near Attack Conformations (NAC). In our previous studies,^{29–31} several models have been suggested to explain the mechanism of deamidation. In these studies, a small model was designed, and calculations have been carried out by using the B3LYP/6-31+G(d) methodology. The mechanisms depicted in Scheme 1 can be classified as follows:

- (A) Direct hydrolysis of asparagine to aspartate (Asn…Asp, black route in Scheme 1).
- (B) Succinimide-mediated deamidation of asparagine to aspartate (Asn…suc). This mechanism is suggested to proceed in three different ways.

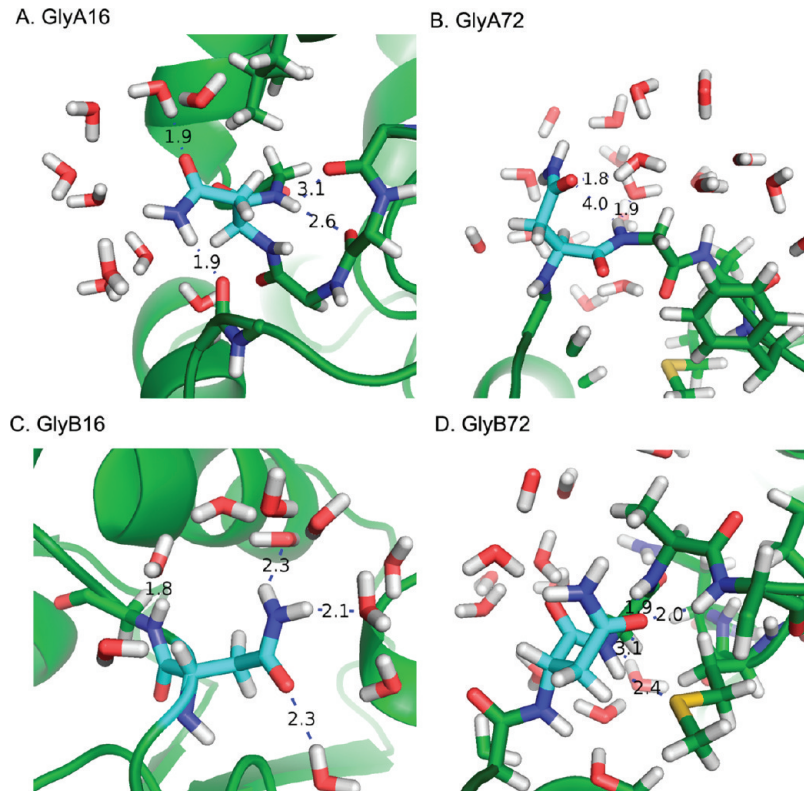


Figure 9. Gly H Interactions, WOW, at 34 ns. (A) GlyA16@H (distance between GlyA16@H and the closest H acceptor is 2.7 Å), (B) GlyA72@H, (C) GlyB16@H, and (D) GlyB72@H.

- (1) One-step mechanism (Asn…suc, green route in Scheme 1).
- (2) Two-step mechanism (Asn…tet…suc, blue route in Scheme 1) via the formation of a tetrahedral intermediate.
- (3) Three-step mechanism where tautomerization of the Asn residue is followed by a tetrahedral intermediate (Asn…taut…tet…suc, red route in Scheme 1).

The catalytic effect of water molecules has been taken into account in all of these mechanisms by introducing explicit water molecules (one or two) and the outcome of these studies can be summarized as follows:

Water assistance increases the rate of deamidation.

The tautomerization route has the lowest barrier for the formation of the succinimide intermediate regardless of the number of water molecules that assist the reaction, including the waterless mechanism.

Cyclization is the rate-determining step for succinimide formation in all water-assisted mechanisms.

For all mechanisms, intermediate and transition state structures have been determined.

One way to analyze our TPI simulations is to check if conformations of the deamidation sites geometrically closed to one of all possible reactant structures can be observed along the trajectories. From Scheme 1 and refs 29–31, one can extract near-attack conformations (NAC) that are depicted in Scheme 2. They correspond to the initial intermediates occurring for the four classes of all possible deamidation reactions (respectively, Asn…Asp, Asn…suc, Asn…tet…suc, and Asn…taut…tet…suc). In each class, reactions can be assisted by, respectively, 0, 1, or 2

water molecules, except for the direct hydrolysis mechanism Asn…Asp.

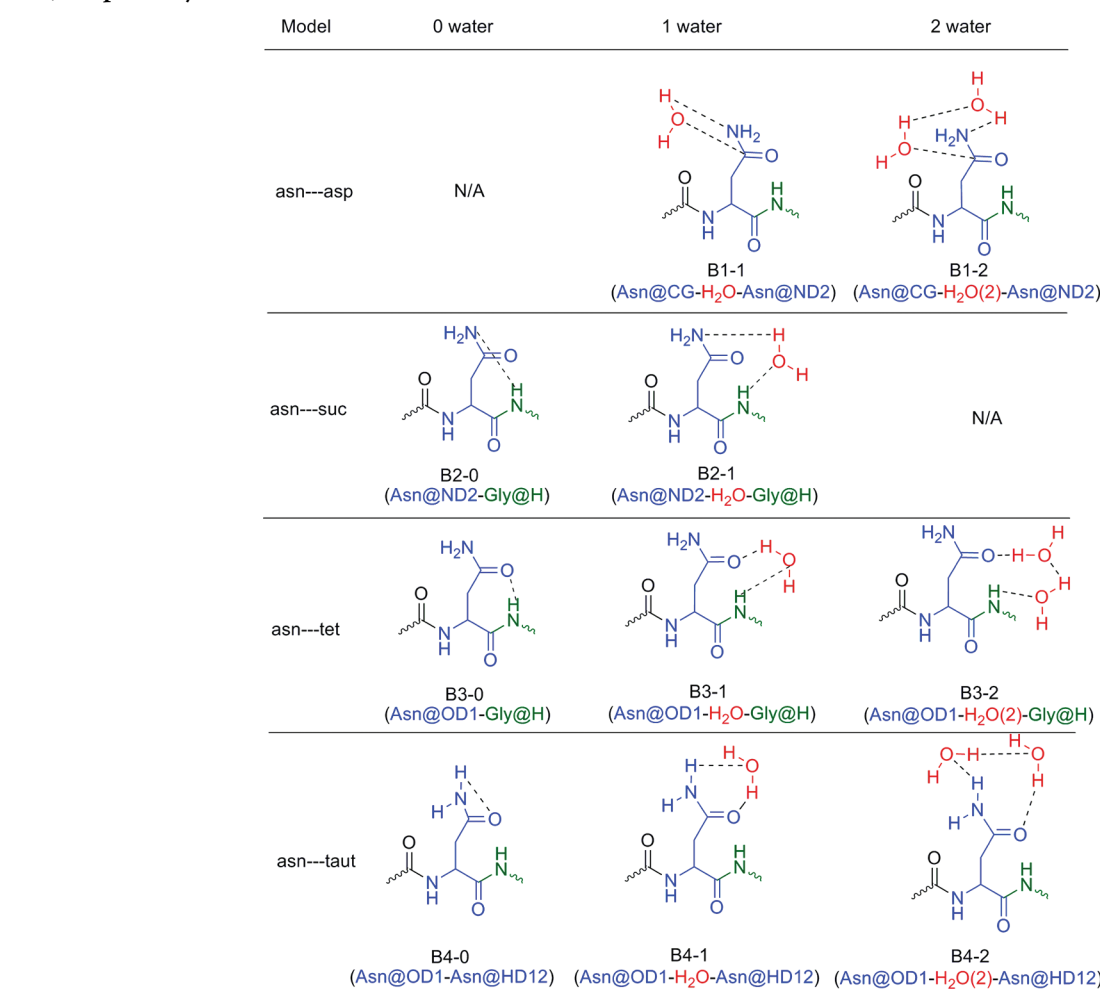
For comparison purposes, in addition to the TPI MD simulations mentioned above, an additional MD simulation has been carried out for a pentapeptide Gly–Gly–Asn–Gly–Gly in a water box environment during 100 ns, using a similar simulation protocol as for the TPI MD simulations.

All trajectories are analyzed in terms of geometrical criteria: intermolecular distances, angles, etc. (see Supporting Information for details), and if occurring, near-attack conformers are identified and assigned to one of the corresponding reactant structures. Figure 10 reports the percent occurrences of favorable interactions during the different simulations.

Previous QM studies on model peptide have evaluated the energy barriers for such reactions.³¹ For the nonassisted tetrahedral intermediate formation, the barrier is estimated at 49.7 kcal/mol, while the two water-assisted tautomerization routes have two consecutive barriers: respectively, 18.1 kcal/mol to form the tautomer and 39.7 kcal/mol to continue up to the tetrahedral intermediates.³¹

In all of the samples, there is nearly no occurrence for the near-attack conformation corresponding to the direct hydrolysis, and the direct formation of a succinimide intermediate. This supports the finding of the previous QM studies: not only do these reactions have higher barriers than the one corresponding to the water-assisted tetrahedral intermediate formation or the water-assisted Asn side chain tautomerization, respectively, but the conformation corresponding to geometries close to the initial reactant states of these difficult reactions do not occur frequently. As a consequence, in TPI, direct hydrolysis and direct succinimide formation are two model deamidation mechanisms that can be ruled out.

Scheme 2. Representations of Models Suggested by QM Studies Asn, Gly, and Water Molecules Are Shown in Blue, Green, and Red, Respectively



In addition, all TPI simulations reveal that NACs occur mostly for two reaction mechanisms: the direct formation of a tetrahedral intermediate (B3-0) and the Asn side chain tautomerization assisted by two water molecules. This suggests that the experimentally observed succinimide intermediate is formed after the formation of a metastable tetrahedral intermediate that can be obtained either directly or through a prior water-assisted tautomerization route (see Scheme 1).

Finally, Figure 10 can be analyzed in terms of differences between primary and secondary deamidation sites. We have not found any obvious pattern differentiating these two sites. At first glance, our results do not suggest that one site could initiate deamidation faster than another by forming more preferentially NACs, as compared to the other deamidation sites.

4. CONCLUSIONS

We have performed molecular dynamics simulations of six possible samples for triosephosphate isomerase: wild-type protein extracted from crystallographic structure (WOW); substrate-bound system (CS); modeled structures to represent closed and open states of TPI (respectively, CC and OO); mutated simulations where the asparagine of the primary deamidation site has been replaced by aspartate residue on each TPI monomer (respectively, AASP and BASP).

Analysis of the trajectories has been performed in terms of (i) global and local desolvation states for each deamidation site;

(ii) hydrogen bond patterns; and (iii) near attack conformations. By using NAC analysis, we have found that only two initiations of the deamidation reaction seem possible in TPI: (1) a mechanism starting with the tautomerization of Asn side chain assisted by two water molecules; (2) a mechanism involving the direct formation of the tetrahedral intermediate.

In each case, the first intermediate formed by the reaction will be a metastable intermediate according to the relative energies reported by Catak et al.^{29–31} However, QM modeling have found that the tautomerization mechanism involved a lower TS barrier than the direct tetrahedral intermediate formation. Because NAC probabilities for the two mechanisms have been found similar, we can hypothesize that the kinetics involving the formation of the tautomer interaction will be faster than the one leading to the direct tetrahedral intermediate formation.

Comparison with a MD simulation of the Gly–Gly–Asn–Gly–Gly pentapeptide shows that NAC probabilities related to the tautomerization reaction as well as the tetrahedral intermediate formation are similar for TPI and the pentapeptide.

However, Gly@H solvent exposures are very different between the pentapeptide and the enzyme. This means that, after the tautomer or the tetrahedral intermediate has been formed, the NH group of the glycine in the pentapeptide will be more easily involved in the deamidation reaction to form either a tetrahedral intermediate or a succinimide intermediate. The metastable intermediate has more chance to go backward to Asn

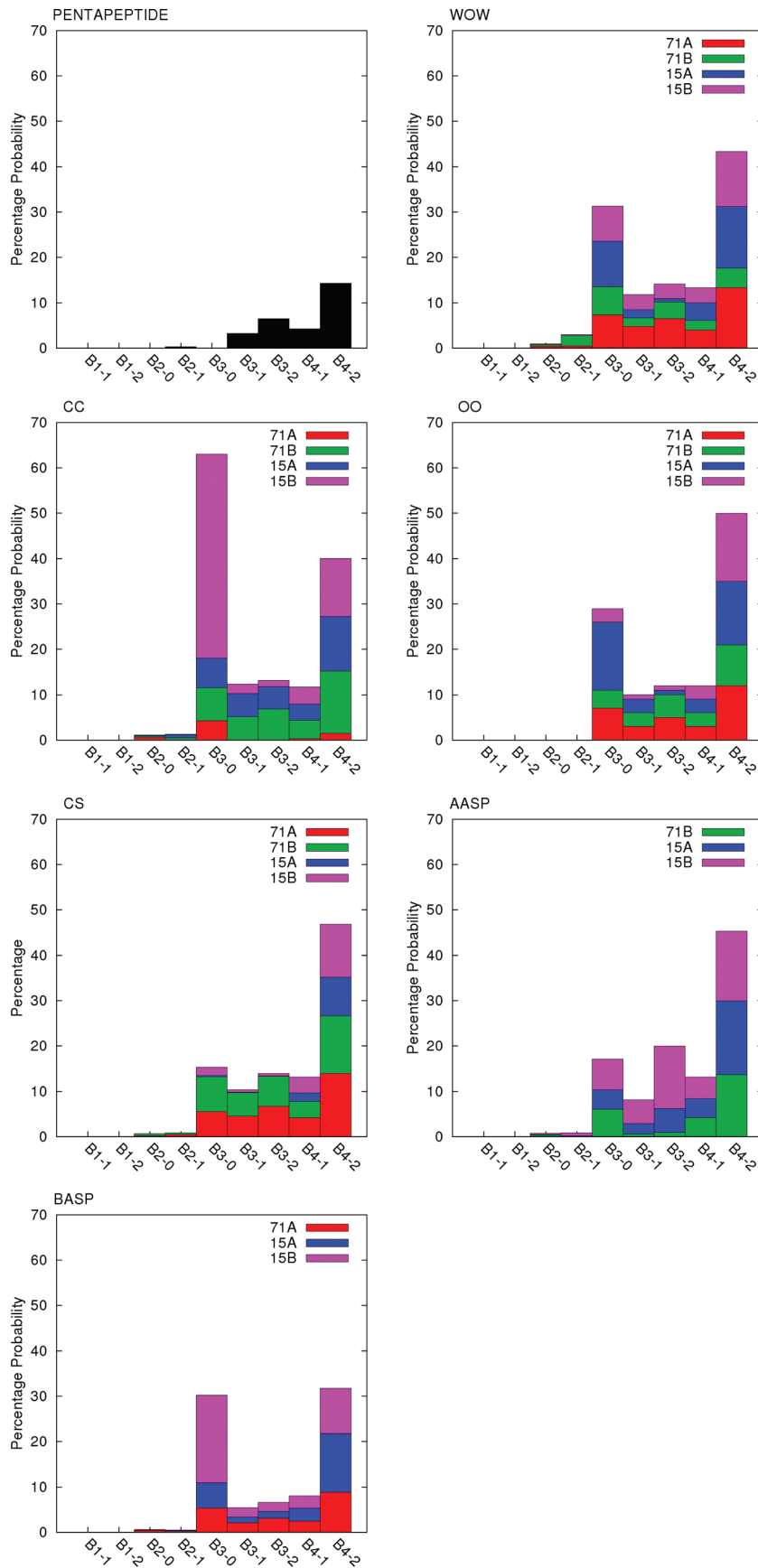


Figure 10. Percent occurrence of the interactions during the simulation. (Number of water molecules within the hydrogen bond network is shown as -0 , -1 , and -2 for the corresponding model.)

in TPI, whereas it will more likely go in the forward direction to form the succinimide intermediate in Gly–Gly–Asn–Gly–Gly. This should explain why experimentally TPI deamidates slower than the pentapeptide.

Experimental studies indicated that Asn71 deamidates faster than Asn15.²⁵ NAC analyses show that Asn71Gly72 and Asn15Gly16 have almost the same probabilities to be found as a reactive conformer. However, NAC analyses have an interest only in the initiation of the deamidation reaction. To fully accomplish the deamidation, two main steps are required: (1) removal of Gly@H to obtain a succinimide intermediate and (2) hydrolysis of succinimide intermediate to aspartate (Scheme 1). Assistance of water is crucial in both steps because of particular reasons. In the first step, water facilitates the reaction as suggested by QM studies. In the second one, the presence of water is mandatory as a reactant. When these facts are considered all together, it can be concluded that more solvated residues should undergo deamidation easier. Desolvation results show that Asn71Gly72 always has higher probability to be in water environment. So, we suggest that Asn71Gly72 will deamidate faster than Asn15Gly16 because of the differences in desolvation results, even though they both can accomplish the reactive conformers.

Another experimental finding is that deamidation of Asn71 is a prerequisite of the deamidation of Asn15.²⁵ Analyses of the trajectories related to N71D mutation in TPI do not lead to clear findings. In the time scale of our simulation, we have not found strong effect of the presence of charged aspartate residue on the structural network around its juxtaposed Asn15. NAC analyses in all the trajectories also show that probabilities for both residues are almost the same.

One of the ultimate goals of the project was to analyze the relationship between the catalytic activity and the motion of the active site loop (loop6) with the deamidation. We have not found any clear evidence of the influence of the loop6 and the substrate at the time scale of the simulations. Although different behaviors are observed in each of the samples, these behaviors cannot be related to the motion of loop6.

■ ASSOCIATED CONTENT

Supporting Information

Variations of the rmsd, atomic fluctuations, N_{15.5} Å data, hydrogen bond occupancies for all samples, and near attack conformer geometrical definitions. This material is available free of charge via the Internet at <http://pubs.acs.org>.

■ AUTHOR INFORMATION

Corresponding Author

*E-mail: Gerald.Monard@univ-lorraine.fr.

Notes

The authors declare no competing financial interest.

■ ACKNOWLEDGMENTS

This research was supported by the TUBITAK-CNRS project (Project No. TUB-108T870). V.A. acknowledges the support of the TUBITAK project 109T862. Computational resources were provided by CINES (Centre Informatique National de l'Enseignement Supérieur) using Grant 2010-076049. I.U. acknowledges a cotutelle grant from the French Embassy in Ankara, Turkey.

■ REFERENCES

- (1) Robinson, A. B.; Rudd, C. *Curr. Top. Cell Regul.* **1974**, *8*, 247–295.
- (2) Robinson, A. B.; Scotthler, J. W.; McKerrow, J. H. *J. Am. Chem. Soc.* **1973**, *95*, 8156–8159.
- (3) Bornstein, P.; Balian, G. *J. Biol. Chem.* **1970**, *245*, 4854–4856.
- (4) Geiger, T.; Clarke, S. *J. Biol. Chem.* **1987**, *262*, 785–794.
- (5) Meinwald, C. Y.; Stimson, E. R.; Scheraga, H. A. *Int. J. Pept. Protein Res.* **1986**, *28*, 79–84.
- (6) Takamoto, L.; Boyle, D. *Mol. Vision* **2000**, *6*, 164–168.
- (7) Watanabe, A.; Takio, K.; Ihara, Y. *J. Biol. Chem.* **1999**, *274*, 7368–7378.
- (8) Weintraub, S. J.; Manson, S. R. *Mech. Ageing Dev.* **2004**, *125*, 255–257.
- (9) Robinson, N. E.; Robinson, A. B. *Proc. Natl. Acad. Sci. U.S.A.* **2001**, *98*, 944–949.
- (10) Capasso, S.; Mazzarella, L.; Sica, F.; Zagari, A.; Salvadori, S. *J. Chem. Soc., Perkin Trans. 2* **1993**, 679–682.
- (11) Capasso, S.; Mazzarella, L.; Sica, F.; Zagon, A. *J. Pept. Res.* **1989**, *2*, 195–197.
- (12) Capasso, S.; Salvadori, S. *J. Pept. Res.* **1999**, *54*, 377–382.
- (13) Tam, J. P.; Riemen, M. W.; Merrifield, R. B. *J. Pept. Res.* **1988**, *1*, 6–18.
- (14) Robinson, N. E.; Robinson, Z. W.; Robinson, B. R.; Robinson, A. L.; Robinson, M. R.; Robinson, A. B. *J. Pept. Res.* **2004**, *63*, 426–436.
- (15) Robinson, N. E.; Robinson, A. B. *J. Pept. Res.* **2004**, *63*, 437–448.
- (16) Robinson, N. E.; Robinson, A. B. *Proc. Natl. Acad. Sci. U.S.A.* **2001**, *98*, 4367–4372.
- (17) Konuklar, F. A.; Aviyente, V.; Sen, T. Z.; Bahar, I. *J. Mol. Model.* **2001**, *7*, 147–160.
- (18) Konuklar, F. A.; Aviyente, V. *Org. Biomol. Chem.* **2003**, *1*, 2290–2297.
- (19) Konuklar, F. A.; Aviyente, V.; Ruiz-Lopez, M. F. *J. Phys. Chem. A* **2002**, *106*, 11205–11214.
- (20) Radkiewicz, J. L.; Zipse, H.; Clarke, S.; Houk, K. N. *J. Am. Chem. Soc.* **1996**, *118*, 9148–9155.
- (21) Radkiewicz, J. L.; Zipse, H.; Clarke, S.; Houk, K. N. *J. Am. Chem. Soc.* **2001**, *123*, 3499–3506.
- (22) Peters, B.; Trout, B. L. *Biochemistry* **2006**, *45*, 5384–5392.
- (23) Wierenga, R. K. *FEBS Lett.* **2001**, *492*, 193–198.
- (24) Pujadas, G.; Palau, J. *Mol. Biol. Evol.* **2001**, *18*, 38–54.
- (25) Gracy, R. W.; Yuan, P. M. *Fed. Proc.* **1980**, *39*, 1690.
- (26) Yuan, P. M.; Talent, J. M.; Gracy, R. W. *Mech. Ageing Dev.* **1981**, *17*, 151–162.
- (27) Gracy, R.; Yüksel, Ü. *Arch. Biochem. Biophys.* **1986**, *248*, 452–459.
- (28) Tyler-Cross, R.; Schirch, V. *J. Biol. Chem.* **1991**, *266*, 22549–22556.
- (29) Catak, S.; Monard, G.; Aviyente, V.; Ruiz-Lopez, M. F. *J. Phys. Chem. A* **2006**, *110*, 8354–8365.
- (30) Catak, S.; Monard, G.; Aviyente, V.; Ruiz-Lopez, M. F. *J. Phys. Chem. A* **2008**, *112*, 8752–8761.
- (31) Catak, S.; Monard, G.; Aviyente, V.; Ruiz-Lopez, M. F. *J. Phys. Chem. A* **2009**, *113*, 1111–1120.
- (32) Aparicio, J. R.; Ferreira, S. T.; Polikarpov, I. *Mol. Biol.* **2003**, *334*, 1023–1041.
- (33) Jogl, G.; Rozovsky, S.; McDermott, A. E.; Tong, L. *Proc. Natl. Acad. Sci. U.S.A.* **2003**, *100*, 50–55.
- (34) Needleman, S. B.; Wunsch, C. D. *J. Mol. Biol.* **1970**, *48*, 443–453.
- (35) (a) McLachlan, A. D. *Acta Crystallogr., Sect. A: Found. Crystallogr.* **1982**, *38*, 871–873. (b) Martin, A. C. R. ProFit. <http://www.bioinf.org.uk/software/profit/>.
- (36) Case, D. A.; Cheatham, T. E.; Darden, T.; Gohlke, H.; Luo, R.; Merz, K. M.; et al. *J. Comput. Chem.* **2005**, *26*, 1668–1688.
- (37) Duan, Y.; Wu, C.; Chowdhury, S.; Lee, M. C.; Xiong, G.; Zhang, W.; Yang, R.; Cieplak, P.; Luo, R.; Lee, T. *J. Comput. Chem.* **2003**, *24*, 1999–2012.
- (38) Jorgensen, W. L.; Chandrasekhar, J.; Madura, J. D.; Impey, R. W.; Klein, M. L. *J. Chem. Phys.* **1983**, *79*, 926–935.
- (39) Andersen, H. C. *J. Chem. Phys.* **1980**, *72*, 2384–2393.

- (40) Essman, U.; Perera, L.; Berkowitz, M. L.; Darden, T. A.; Lee, H.; Pedersen, L. G. *J. Chem. Phys.* **1995**, *103*, 8577–8593.
- (41) Ryckaert, J. P.; Ciccotti, G.; Berendsen, H. J. C. *J. Comput. Phys.* **1977**, *23*, 327–341.
- (42) Williams, T.; Kelley, C.; et al. Gnuplot. <http://www.gnuplot.info>.
- (43) Sertan, C.; Doruker, P. *Biochemistry* **2008**, *47*, 1358–1368.
- (44) Wierenga, R. K.; Kapetaniou, E. G.; Venkatesan, R. *Cell. Mol. Life Sci.* **2010**, *67*, 3961–3982.
- (45) Li, H.; Robertson, A. D.; Jensen, J. H. *Proteins: Struct., Funct., Bioinf.* **2005**, *61*, 704–721.